Direct Numerical Simulation of Airfoil Separation Bubbles

Ulrich Maucher, Ulrich Rist and **Siegfried Wagner** [1]

Abstract. In the present paper results of Direct Numerical Simulations of Laminar Separation Bubbles caused by streamwise increasing pressure gradient are shown. Small amplitude random disturbances are strongly amplified and therefore the flow shows unsteady behaviour. The spatial growth of the disturbances and the corresponding velocity profiles derived by Fourier transform are compared with results of linear stability theory (so-called Tollmien-Schlichting waves (TS-waves)). Cases with and without artificial disturbances are considered. Two major time scales are observed. The first one is corresponding to the hydrodynamic instability (TS-waves), while the second, large one, is associated with an oscillation of the bubble and occurs in undisturbed cases. The damping influence of an upper boundary condition in the numerical domain with interaction between the viscous boundary layer and the inviscid outer flow (interaction model) on this large-scale effect is also shown.

1 INTRODUCTION

When a laminar boundary layer is subjected to an adverse pressure gradient it will eventually separate. As the separated boundary layer resembles a free shear layer which is known to be very unstable with respect to a broad spectrum of disturbances the flow will most probably become turbulent. Turbulence, in consequence, will entrain high-momentum fluid from the outer part of the separated flow towards the wall and will cause re-attachment in many cases. Such a phenomenon where a closed reverse-flow region exists at the wall is termed a *Laminar Separation Bubble* (LSB). The involved flow physics are not yet fully understood. Since flight performance characteristics of laminar airfoils and compressor blades strongly degrade with the existence of laminar separation bubbles there is great interest in further investigations.

2 NUMERICAL METHODS

Here the computational techniques used for the present investigations are introduced. The calculations in this paper are based on two approaches, Direct Numerical Simulation (DNS), and Linear Stability Theory (LST) [6]. Both methods have already been discussed in the literature. Therefore, only the essentials are outlined here. To extract basic features of the DNS-results Fourier Transform is used.

[1] Universität Stuttgart, Institut für Aerodynamik und Gasdynamik, Pfaffenwaldring 21, 70550 Stuttgart, Germany

ECCOMAS 94.
Published in 1994 by John Wiley & Sons, Ltd.

2.1 Direct Numerical Simulation

The calculations presented in this paper are performed with a numerical scheme originally developped by Fasel et al. [2], improved by Kloker [4] and more recently by Kloker et al. [5]. The method is based on the complete Navier-Stokes equations in vorticity-velocity formulation for unsteady, three-dimensional, incompressible flow. Since the major changes of the code deal with features which are used to calculate the two-dimensional (2-D) component of the flow, this paper is restricted to 2-D flows. Consequently, only the equations for the 2-D components will be explained in this section. The velocity components are denoted by u in streamwise (x) and v in wall-normal direction (y) (see figure 1).

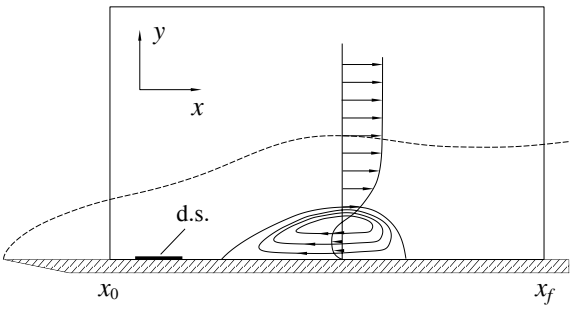

Figure 1. Integration domain for the DNS of a LSB; d.s.: disturbance strip.

All variables are nondimensionalized with a reference length L and the free stream velocity U_∞. The nondimensional variables relate to the corresponding dimensional ones (denoted by bars) as

$$x = \frac{\bar{x}}{L}, \quad y = \frac{\bar{y}}{L}\sqrt{Re}, \quad t = \bar{t}\frac{U_\infty}{L}, \qquad u = \frac{\bar{u}}{U_\infty}, \quad v = \frac{\bar{v}}{U_\infty}\sqrt{Re}, \quad Re = \frac{U_\infty L}{\bar{\nu}}, \tag{1}$$

where $\bar{\nu}$ is the kinematic viscosity and Re is the Reynolds number. The vorticity is defined as

$$\omega = \frac{\partial u}{\partial y} - \frac{1}{Re}\frac{\partial v}{\partial x}. \quad (2)$$

In contrast to the disturbance-flow formulation used by Kloker [4][5] (i.e. the flow is split into a steady base-flow and an unsteady disturbance-flow), now the total-flow formulation is used, since a solution for a steady base flow cannot be obtained due to the high amplification rates of random disturbances in the separated flow considered here. Thus the vorticity-transport equation (3), the Poisson-equation (4) and the equation for continuity (5) have to be solved to obtain ω, v, and u, respectively:

$$\frac{\partial \omega}{\partial t} + \frac{\partial}{\partial x}(u\omega) + \frac{\partial}{\partial y}(v\omega) = \frac{1}{Re}\frac{\partial^2 \omega}{\partial x^2} + \frac{\partial^2 \omega}{\partial y^2}, \quad (3)$$

$$\frac{1}{Re}\frac{\partial^2 v}{\partial x^2} + \frac{\partial^2 v}{\partial y^2} = -\frac{\partial \omega}{\partial x}, \quad (4)$$

$$\frac{\partial u}{\partial x} = -\frac{\partial v}{\partial y}. \quad (5)$$

For discretisation of the governing equations in streamwise and wall-normal direction, central finite-differences of fourth-order-accuracy are used. The integration in time is performed with a fourth-order accurate Runge-Kutta scheme. The four stages per time step of this scheme are coupled with a centered-upwind-downwind-(and vice versa)-centered discretisation for the x-convection term.

Optionally, the flow can be disturbed by time-periodic suction and blowing within a so called *Disturbance Strip* on the surface of the plate (figure 1). In that way, TS-waves with prescribed frequency and amplitude can be generated (see [5] for details). In x-direction the integration domain extends from x_0 to x_f and covers a certain region of the boundary layer flow over an airfoil including a laminar separation bubble, while in y-direction the domain typically covers approximately 10 displacement thicknesses at the inflow boundary.

At the free-stream boundary a streamwise pressure gradient is imposed by prescribing the free-stream velocity distribution $u_e(x)$ of the external flow, assuming inviscid flow. For the simulations discussed in this paper $u_e(x)$ is chosen to approximate the potential flow distribution from s/c=0.215 to s/c=0.578 on the upper side of an FX66-S-196 airfoil at 9 degrees angle of attack (see figure 2a), as obtained from an experiment. The vorticity is set to zero.

At the inflow boundary, steady flow is assumed. An approximated Hartree-parameter β_H calculated from the local slope of the u_e velocity at the inflow boundary is used to calculate Falkner-Skan profiles.

At the outflow boundary a new condition based on the so-called *Relaminarisation Zone* technique, a special buffer domain developed and extensively tested by Kloker et al. [5] is introduced. Now, the total 2-D vorticity is artificially damped to 0 by multiplying it with a function which smoothly decays

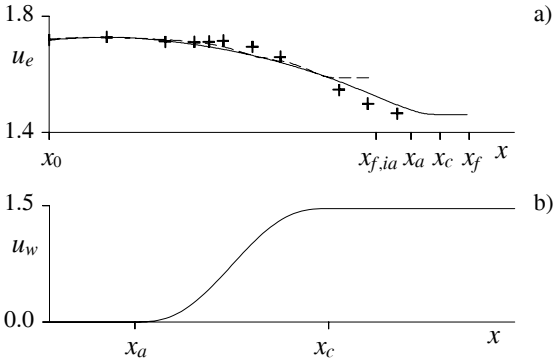

Figure 2. a) Velocity distribution (u_e) at the free-stream boundary. x_a denotes the beginning of the region with acceleration at the wall and x_c constant u velocity. The dashed line shows the data with interaction (ia) at the upper boundary, crosses mark experimental data.
b) Velocity distribution (u_w) at the wall.

from 1 to 0 near the outflow boundary. In addition, the free-stream u-velocity is set to a constant value and the velocity at the wall is accelerated to its free stream value (see figure 2b). This leads to uniform and irrotational flow throughout the boundary layer. This new method has been rigorously tested for spatially evolving TS waves in Blasius flow (§ 3), its applicability for laminar separation bubbles is shown in the present paper (§ 4).

To take the displacement effect of the separation bubble on the potential flow into account, a model for viscous-inviscid interaction developed by Gruber [3] based on thin-airfoil theory can be used optionally. The v-velocity v_e at the free-stream boundary is split into an inviscid component V and a part v_c related to displacement

$$v_c = v_e - V = v_e + y_e\frac{dU}{dx}, \quad (6)$$

where V has been replaced by the prescribed potential flow distribution U using the continuity equation (5). U in the present case coarsly approximates the potential flow over an FX66-S-196 airfoil (figure 2a). Now u_e can be updated from

$$u_e = U + \frac{1}{\pi}\int_{\xi=x_l}^{x_r}\frac{v_c}{x-\xi}d\xi, \quad (7)$$

where x_l, and x_r are the left, and the right boundary, respectively, where displacement effects of the boundary layer and especially the bubble are considered. The code neglects curvature of the airfoil since the curvature radius is very large compared to the boundary layer thickness.

To start the simulation, initial values for the whole flowfield are needed. These are taken either from the solution of a boundary-layer calculation, or from the averaged values of a previous simulation with the same boundary-conditions. After a period of transient behaviour the appearance of a 'quasi-periodic' state of the flow is observed.

2.2 Linear Stability Theory

In the present paper unsteady flows are investigated. The major interest focuses on the development and the profiles of the disturbances. For the validation of the DNS-results comparisons with results of Linear Stability Theory (LST) can be used. For the LST calculations local velocity profiles of a steady base flow are needed. As for the simulations discussed in this paper no steady base flow exists, the stability calculations are performed for the mean base flow profiles generated by averaging the DNS velocity components over a long time. The local streamwise variation of the base flow is neglected in the theory. Thus uniform steady 2-D base flow is assumed locally and the profiles depend on y only. Disturbances of the form

$$v'(x,y,t) = A(y)e^{-\alpha_i x}\cos(\alpha_r x - \beta t - \Theta(y)) \qquad (8)$$

are considered, where v', A, α_i, α_r, β, and Θ denote a velocity-component of the wave, amplitude, spatial amplification rate, streamwise wave number, frequency, and phase, respectively. Negative α_i means amplification in x-direction.

This ansatz is inserted into the Navier-Stokes equation. Linearisation then yields the so-called Orr-Sommerfeld equation. From the solution of the Orr-Sommerfeld equation eigenfunctions (disturbance velocity profiles) and amplification rates for given base-flow velocity profiles, Reynolds number, and frequency, are obtained.

2.3 Fourier Transform

Fourier analysis yields the complex amplitudes of the frequency spectrum of a periodic signal [1]. Since all DNS cases presented in this paper are unsteady, an important attempt to understand and validate results is Fourier Analysis. The following discrete ansatz defines the Fourier Transform (FT) that is used

$$F(x,y,\frac{n}{L\Delta t}) = \Delta t \sum_{k=0}^{L-1} f(x,y,t_1 + k\Delta t)e^{-i\frac{2\pi nk}{L}}, \qquad (9)$$

where f, Δt, t_1, F, L, n denote the waveform to be decomposed into a sum of sinusoids, the time step, the initial point of the analyzed time window, the complex Fourier amplitude, the number of discrete points (in time) and an integer counting the frequency β as follows:

$$\beta = \frac{2\pi n}{L\Delta t}. \qquad (10)$$

If a function is not periodic or if the arbitraryly chosen time window $L\Delta t$ does not consist of an integer multiple of the period, 'noise' is introduced into the spectrum by the FT. This is particularly apparent if there is a large discrepancy between the starting and end point of the interval. Especially in strong unperiodic DNS cases it is often difficult to determine a time window in such a way, that results of FT are meaningful and independent of the choice of the time window. Using a Hanning window to modify the time signal before applying FT may help to reduce such undesirable effects:

$$f_h(t) = f(t)\left[0.5 - 0.5\cos\left(2\pi\frac{t-t_1}{t_2-t_1}\right)\right]. \qquad (11)$$

3 VERIFICATION OF THE PARALLEL-OUTFLOW CONDITION

To validate the parallel-outflow condition, test calculations for the well known Blasius flow with artificially excited disturbances have been performed. The base flow is described by $Re = 10^5$, $U_\infty = 30\frac{m}{s}$, $\bar{\nu} = 1.5 * 10^{-5}\frac{m^2}{s}$, $L = 0.05m$. The frequency of the disturbances is $\beta_t = 11$. The spatial development of the excited small-amplitude TS-waves is compared with results of LST in figure 3. The amplification rates for the u-velocity maximum normal to the wall derived from DNS and the respective results from LST are shown. Excellent agreement between both approaches is observed. There is almost no upstream influence of the parallelization zone. Even at the beginning of the acceleration of u at the wall, the amplification rates agree well. Since amplification rates are very sensitive even to slight variations of the base flow, the results demonstrate the suitability of the parallel-outflow boundary condition.

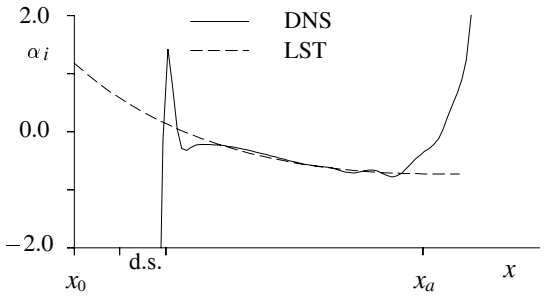

Figure 3. Amplification rates $\alpha_i = -\frac{\partial}{\partial x}\ln(u'_{max})$ compared with LST for Blasius flow.

4 RESULTS FOR FLOWS WITH SEPARATION

So far, only 2-D simulations for flows with strong adverse pressure gradient and a separation bubble have been performed with the new code. The velocity distribution u_e prescribed at the free-stream boundary is taken from an experiment for a FX 66-S-196 airfoil at 9 degrees angle of attack and a chord-Reynolds number of Re=1.5 * 10^6 (see figure 2a). A case with fixed velocity u_e at the upper boundary and without artificial disturbances is investigated extensively. Furtheron the influence of the IA-model at the upper boundary and the development of artificial disturbances is briefly presented.

All DNS are performed using Re=1.5 * 10^5, U_∞=30.28$\frac{m}{s}$, $\bar{\nu} = 1.5 * 10^{-5}\frac{m^2}{s}$, $L = 0.0743m$. The integration domain extends from x_0 = 2.153 (c/s=0.215) to x_f = 5.782 (c/s=0.578; in

cases with interaction x_f = 4.977, c/s=0.498) with 722 (562) grid points and from y=0 to y=48.19 with 97 grid points ($\Delta x = 5.034 * 10^{-3}$, $\Delta y = 0.5020$). In the case of artificially excited disturbances the frequency of the disturbances is chosen to be $\beta_t = 30$.

4.1 Results for fixed u_e, self-excited disturbances

The simulation was started using the averaged flow fluid data from a previous simulation as initial condition. The initial transient stage of development was terminated at approximately t=16.76=t_{tr}. For t>t_{tr} a 'quasi-periodic' behaviour of the flow field was observed, as discussed subsequently.

An overall impression of the flow-field at $t - t_{tr}$=2.72 can be obtained from figure 4, where lines of constant velocity component u are shown. Although steady inflow and free-stream boundary conditions are used, the flow exhibits large-amplitude unsteady disturbances and remains unsteady for all times. Due to the parallel-outflow condition at the end of the integration domain, all fluctuations of the u-component disappear. A distinct separation bubble is visible through the reverse flow region. Downstream of the bubble, strong variations of u in streamwise direction are apparent. Since there are no artificial disturbances, these fluctuations indicate the appearance of self-excited wave packets, possibly due to the strong instability of the separated flow.

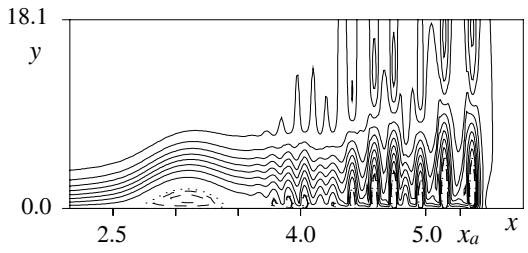

Figure 4. Fixed u_e: u = -0.04, -0.02 (dashed), 0 (dotted), 0.2, 0.4, ... , 1.6 (solid).

In figure 5 the instantaneous time signals for the vorticity at the wall at different downstream positions are plotted versus $t - t_{tr}$. In addition to the high-frequency disturbances corresponding to the wave packets in figure 4, a low frequency oscillation appears, especially in the region near the inflow boundary (i.e. at x=3.0 and x=3.5 in figure 5). The low frequency oscillation lets the separation bubble periodically appear and disappear (note that negative vorticity at the wall corresponds to reverse flow, i.e., separation). The high-frequency oscillations are compared with results from LST in the following section.

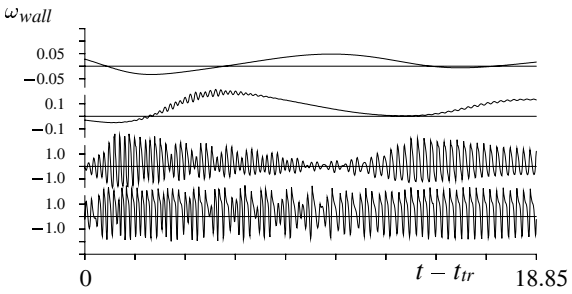

Figure 5. Fixed u_e: Time signals at different downstream positions (x=3.0 (top), x=3.5, x=4.0, x=4.5).

4.1.1 Comparison with LST

Results from a Fourier analysis of the wall-vorticity time signals as plotted in figure 5 are shown in figure 6. Starting at x=3.0 a remarkable amplitude is observed only for very low frequencies. However, the frequencies about β=23 and β=30 exceed the surrounding amplitudes. Further downstream (x=3.5) a frequency hillock appears between $\beta \approx 20$ and $\beta \approx 32$ with amplitudes that are more than two magnitudes larger than other frequencies (except the very low ones). The large-amplitude frequency-band strongly grows in downstream direction and as it gains large amplitudes, other frequencies are also strongly amplified (x=3.75, x=4.0, x=5.0).

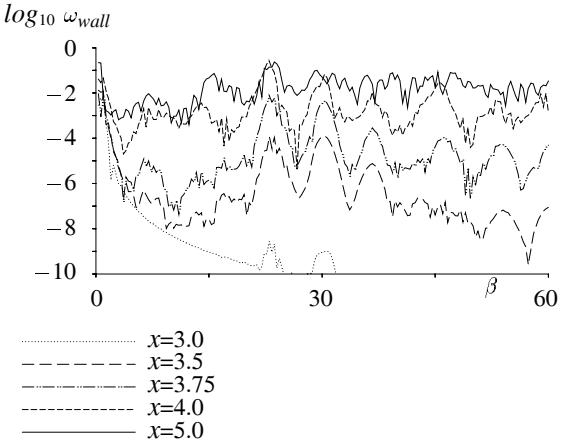

Figure 6. Fixed u_e: u' amplitude-spectrum.

The amplification of each frequency component can be determined by calculating its amplification rate $\alpha_i = -\frac{\partial}{\partial x} \ln \frac{u'}{u_e}$ which in turn is comparable with LST. In the present case, however, due to the self-excited nature of the disturbances, these amplification rates show large-amplitude random oscillations, and a comparison of α_i with LST is difficult. We therefore show a comparison of u'-velocity profiles in figure 7. The time window used to generate the u'-profiles as well as the av-

eraged base flow for LST extends from $t - t_{tr}$=20.94 to 23.04. The comparison is performed for the frequency β=18. Initially (x=3.0) the disturbance amplitude is very small ($\mathcal{O}(10^{-8})$) and the DNS profile resembles more to the base flow profile than to the LST-eigenfunction. With increasing x, however, the disturbance profile continuously changes from its initial shape towards the shape of a TS-wave. Especially at x=4.0 the agreement with LST is very good. Further downstream, the profiles start to differ, but this can be attributed to nonlinear effects due to the large disturbance amplitude of the waves in the DNS which in addition to changing the disturbance profiles feed energy into higher harmonics (waves with a multiple of the fundamental frequency).

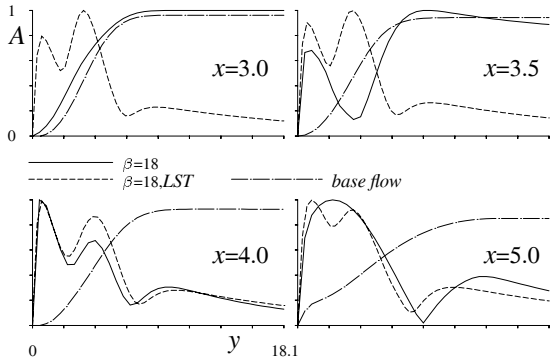

Figure 7. Fixed u_e, self-excited disturbances: u'-profiles. A denotes $\frac{u'_\beta}{u'_{\beta,max}}$.

The phase Θ of the frequency β=30 of the vorticity at the wall versus x is plotted in figure 8. The analyzed time interval corresponds to the interval shown in figure 5.

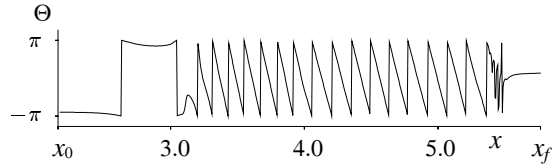

Figure 8. Fixed u_e, self-excited disturbances: Phase Θ of the disturbance mode β=30 of the vorticity at the wall.

There are three different zones. Near the inflow boundary there are only slight variations of the phase with a large wavelength. This can be explained with the low frequency oscillation of the bubble. Figure 5 shows that the phase of the low-frequency oscillations differs at different x-positions (x=3.0 and x=3.5). In the domain where TS-waves are dominant the phase has the typical shape for propagating waves (continuously decreasing). Near the outflow boundary the TS-waves are strongly damped and consequently the phase approaches a constant value, which is different from the value at the inflow boundary. Therefore, pressure disturbances which possibly could be generated by the outflow-boundary and then propagate upstream with infinite velocity (in incompressible flow i.e. constant phase) seem not to have remarkable impact on the development of disturbances in the present code.

4.1.2 Low frequency bubble oscillation

In the region between x=2.8 and x=3.7 the flow periodically separates and reattaches. The condition with fixed u-velocity at the upper boundary is not able to take displacement effects caused by the bubble into account. In real flows the displacement effect of a growing bubble leads to an acceleration of the outer flow and reduction of the adverse pressure gradient and consequently to a decrease of the bubble. On the other hand this decelerates the outer flow and promotes separation. Both adverse effects stabilize each other. Regarding the long-time behaviour it seems that the bubble oscillations slowly decay. The simulation has been stopped at $t - t_{tr}$=23.04 and it is not certain if the low frequency oscillations would completely disappear for larger simulation time. Effects comparable to the bubble oscillation in the present simulation have been observed in previous 2-D simulations of flat-plate separation bubbles [3] or backward facing steps in channel flow. Possibly there is no solution for the steady base flow for some 2-D problems.

4.2 Interaction at the upper boundary, self-excited disturbances

In order to suppress the low-frequency bubble oscillation the effect of an alternate upper boundary condition, which considers displacement effects by the bubble was investigated. A condition satisfying all expectations could not be found, yet. The interaction model by Gruber [3] calculates the u_e component by integration in a large x-domain (see eq. (7)) and therefore allows for upstream influence of disturbances which are strongly damped in real flow in upstream direction. This leads to an excitation of disturbances with moderate amplitude at the upper boundary. Nevertheless, calculations using an interaction model show encouraging results since the low-frequency oscillation of the LSB is damped.

Figure 9 shows the amplitude spectrum of the vorticity at the wall. When the interaction model is used, a broad spectrum of disturbances appears in the flow near the inflow boundary (x=3.0). In downstream direction some frequencies are amplified and a hillock appears in the spectrum for frequencies $15 < \beta < 32$ at x=3.5. Higher frequencies are still not amplified in this region. As the fundamental disturbances grow to very large values all frequencies are strongly amplified and gain large amplitudes (x=3.75 and x=4.0).

4.3 Interaction, artificially disturbed

In order to check the accuracy of the present DNS by further comparisons with LST, a case with artificial disturbances has

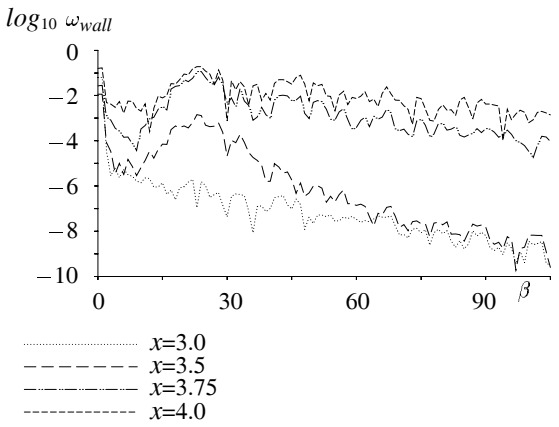

Figure 9. Interaction, self-excited disturbances: ω_{wall} amplitude-spectrum.

been computed. An artificial disturbance with a frequency of β = 30 and an amplitude of u'_{max}=10^{-4} was excited at the disturbance strip located at $2.26 \leq x \leq 2.39$.

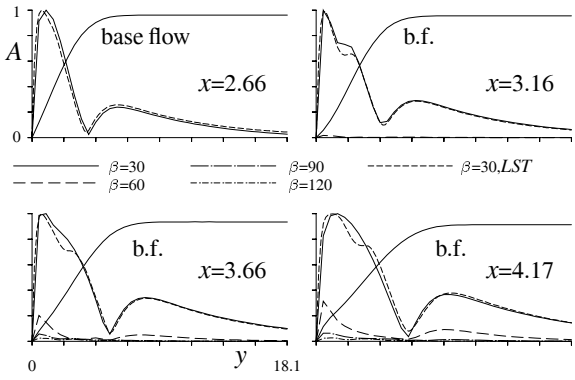

Figure 10. Interaction, artificially disturbed: u'-profiles. A denotes $\frac{u'_\beta}{u'_{\beta=30,max}}$.

Velocity profiles for the u'-component are plotted in figure 10, and compared with the eigenfunctions obtained from LST-analysis for the time-averaged mean-flow profiles at four different x-positions. Every plot contains the profiles of the disturbance wave, its higher harmonics (β=60, 90, 120), the LST-profile, and the local base flow. The first position (x=2.66) is located in a region where the flow is still slightly accelerated and the LST and the DNS profiles fit very well. At the second position (x=3.16) they are very similar with little differences only. These are supposed to be due to the strong non-parallelism of the base flow caused by the deceleration (which is neglected by LST due to the assumption of a locally parallel base flow). In addition, a nonlinear evolution of the disturbance has started: the higher harmonic wave β=60 is amplified and visible in the picture with very low amplitude. Moving further downstream (x=3.66, x=4.17), the DNS profiles differ even more from the LST profiles.

The disturbance amplitudes upstream of the position where the oscillating bubble originally appeared are now larger since the initial amplitude is comparably high. The propagation of energy towards the wall caused by the artificially excited disturbances obviously supresses the process leading to the oscillating bubble. The spectrum (see figure 11) shows the expected shape with strong peaks at the excited frequency and its higher harmonics. On the other hand, it is surprising that at any x-position the amplitudes of the higher harmonics exceed other neighbouring frequencies by far, even when the amplitude of the fundamental wave is comparably low and amplification of the higher harmonics by nonlinear interaction does not take place (x=3.0). Since the unsteady effects are dominated by the excited frequency and its higher harmonics for all x it is very likely that, for the present case, the IA-model propagates discrete frequencies (here the higher harmonics) in upstream-direction.

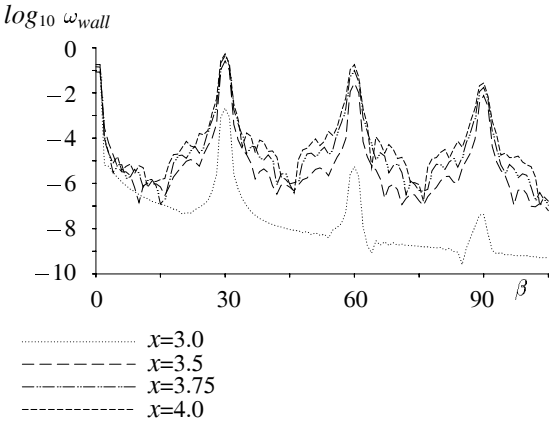

Figure 11. Interaction, artificially disturbed: ω_{wall} amplitude-spectrum.

5 CONCLUSIONS

The results presented in this paper demonstrate that the numerical method can be applied to boundary layer flows with strong adverse pressure gradients including laminar separation bubbles, which, for example, appear on laminar airfoils. The initial 2-D development of TS-waves can be predicted very well. Nevertheless, 2-D simulations neglect a lot of basic features of separated or strongly decelerated flows. The growth of 3-D disturbances has major impact on these flows. Therefore 3-D calculations will be necessary to get better insight into the flow physics of transitional airfoil flows.

ACKNOWLEDGEMENTS

This research is supported by the Deutsche Forschungsgemeinschaft (DFG), Bonn-Bad Godesberg, FRG, under contract Ri 680/1-1.

REFERENCES

[1] E. Oran Brigham, *THE FAST FOURIER TRANSFORM*, Prentice-Hall, Inc., Englewood Cliffs, N.J., 1 edn., 1974.

[2] Hermann Fasel, Ulrich Rist, and Uwe Konzelmann. Numerical investigation of the three-dimensional development in boundary layer transition, 1990.

[3] Karl Gruber. Numerische Untersuchungen zum Problem der Grenzschichtablösung, 1988. Dissertation, Universität Stuttgart.

[4] Markus Kloker. Direkte Numerische Simulation des laminar-turbulenten Strömungsumschlages in einer stark verzögerten Grenzschicht. Dissertation, Universität Stuttgart, 1993.

[5] Markus Kloker, Uwe Konzelmann, and Hermann Fasel. Outflow boundary conditions for spatial Navier-Stokes simulations of transition boundary layers, 1993.

[6] L. M. Mack. Boundary-layer stability theory, 1969.